Diego Carnevale*, Srinivas Chinthalapalli
and Geoffrey Bodenhausen

Exciting Wide NMR Spectra of Static Solid Samples with Weak Radiofrequency Fields

Abstract: Trains of short pulses in the manner of 'delays alternating with nutations for tailored excitation' (DANTE) have been applied to the Pake patterns of protons of water molecules trapped in a static powdered sample of barium chlorate monohydrate. The spin dynamics in the course of such experiments have been investigated by means of numerical simulations and compared with the ideal refocusing that can be achieved under magic-angle spinning (MAS). Solid echoes yield essentially undistorted lineshapes, in contrast to direct excitation without refocusing that leads to severe dispersions of the phases because of inhomogeneous interactions such as homonuclear dipolar couplings and anisotropic chemical shifts. The selectivity of DANTE sequences allows one to access 'slices' of the Pake pattern that can be related to particular crystallite orientations. Single-crystal spectra can therefore be extracted from powder spectra. A similar behavior is expected for both dipolar and quadrupolar echoes.

Keywords: DANTE; dipolar echoes; dipolar interactions; hydration water; NMR spectroscopy; quadrupolar echoes; quadrupolar interactions; solid echoes; solid-state NMR of static samples.

---

*Corresponding author: Diego Carnevale, Neuchâtel Platform of Analytical Chemistry (NPAC), Institut de Chimie, Université de Neuchâtel, Avenue de Bellevaux 51, 2000 Neuchâtel, Switzerland, e-mail: diego.carnevale@unine.ch; and Institut des sciences et ingénierie chimiques (ISIC), Ecole Polytechnique Fédérale de Lausanne (EPFL), 1015 Lausanne, Switzerland
Srinivas Chinthalapalli: Institut des sciences et ingénierie chimiques (ISIC), Ecole Polytechnique Fédérale de Lausanne (EPFL), 1015 Lausanne, Switzerland; and Analytical and Spectroscopy Division (ASD), Analytical, Spectroscopy and Ceramics Group (ASCG), Propellants, Polymers, Chemicals and Materials (PCM) Entity, Vikram Sarabhai Space Centre (VSSC), Thiruvananthapuram 695 022, India
Geoffrey Bodenhausen: Institut des sciences et ingénierie chimiques (ISIC), Ecole Polytechnique Fédérale de Lausanne (EPFL), 1015 Lausanne, Switzerland; Departement de Chimie, Ecole Normale Superieure, PSL Research University, UPMC Univ Paris 06, CNRS, Laboratoire des Biomolecules (LBM), 24 rue Lhomond, 75005 Paris, France; and Sorbonne Universites, UPMC Univ Paris 06, Ecole Normale Superieure, CNRS, Laboratoire des Biomolecules (LBM), Paris, France

1 Introduction

Solid-state NMR is an invaluable tool for the structural characterization of systems where diffraction techniques are less effective due to dynamics or to a lack of long-range order. Valuable insight into dynamic processes such as chemical exchange and molecular reorientation can be obtained. When the interactions that affect nuclear spins in solids are anisotropic [1], this results in static NMR lineshapes commonly referred to as 'powder patterns' that are inhomogeneously broadened. In samples spinning about the magic-angle, the properties of DANTE trains [2, 3] of radiofrequency (rf) pulses applied in a rotor-synchronized fashion have been thoroughly investigated [4–8]. In this paper, we turn our attention to the application of such pulse trains to static samples that are subject to inhomogeneous broadening. DANTE sequences can offer both a uniform broadband excitation extending over several MHz, and the selective excitation of chosen frequency ranges extending over a few kHz. These paradoxical features are particularly appealing to study samples that are subject to large inhomogeneous interactions, such as hyperfine couplings in paramagnetic systems, or dipolar interactions [6, 7]. For the latter interactions, a spin system comprising only isolated pairs of nuclear spins, like water trapped in gypsum ($CaSO_4$) [9] offers an instructive example. We have investigated the protons of water trapped in barium chlorate monohydrate, $Ba(ClO_3)_2.H_2O$ [10]. The distance between the two protons belonging to a given water molecule is ca. 1.6 Å, leading to a homonuclear dipolar coupling constant of ca. 30 kHz, giving rise to a nearly ideal Pake pattern [9]. The distance between two neighboring water molecules in $Ba(ClO_3)_2.H_2O$ is ca. 4.8 Å, resulting in intermolecular dipolar couplings below 1 kHz which barely affect the Pake pattern.

If one combines DANTE pulse trains with sample rotation about the magic angle, there is a synergy between the mechanical rotation, which refocuses the spatial parts of anisotropic interactions of rank 2 (but not of second-order quadrupolar couplings) to form rotational echoes, and the nutation due to the rf pulses that affects the spin part of the interactions [6]. Neglecting homogeneous losses, this allows one to excite a coherence (transverse magnetization) through the cumulative effects of small flip angles in a uniform manner over several MHz, provided all inhomogeneous interactions can be refocused by rotation about the magic angle.

In static samples, on the other hand, there are of course no rotational echoes, and it is far from obvious that the cumulative effects of a train of pulses can excite a coherence. In this study, we investigate some properties of both excitation and refocusing by DANTE pulse trains applied to static samples. The spin dynamics that occur during the pulse trains are analyzed by means of numerical

simulations. The refocusing properties of DANTE echoes in static samples are compared with echoes of equivalent experiments performed under magic-angle spinning (MAS), where full refocusing can be achieved. The comparison serves as a test for our experiments in static samples. Applications to the Pake pattern of $Ba(ClO_3)_2.H_2O$ show how DANTE trains can be used to extract spectra corresponding to single crystals with different orientations with respect to the external magnetic field.

2 Results and discussion

In previous studies we have introduced the nomenclature D_N^K to describe DANTE pulse trains applied to samples that are spinning at the magic angle, N being the number of rf pulses per rotor period and K the number of rotor periods that corresponds to the length of the entire pulse train, which therefore comprises $M = K \times N$ pulse [6]. In static samples, where the concept of a rotor period is meaningless, a DANTE train $[\tau_p^\phi - \tau -]_M$ can simply be described by D_M, M being the number of pulses that constitute the train. In this work, we will use the nomenclature D_M^ϕ where the index ϕ indicates the phase that is common to all rf pulses in the pulse train. By analogy, we will use $D_N^{K,\phi}$ for spinning samples. Figure 1(a) depicts a pulse scheme inspired by the well-known $90_x^\circ - \tau - 90_\phi^\circ - \tau -$ scheme used to excite solid echoes with $\phi = \pi/2$ [11, 12]. By themselves, such experiments cannot simultaneously refocus both linear interactions (chemical shifts) and quadratic interactions (dipolar or quadrupolar couplings) [13]. This can however be achieved by combining a solid echo sequence with a suitable prescription for cycling the phase ϕ [14]. By analogy to the familiar $90_x^\circ - \tau - 90_\phi^\circ - \tau -$ solid echo scheme, one can use a $D_{10}^x - \tau' - D_{10}^\phi - \tau' -$ sequence (or $[\tau_p^x - \tau -]_M - \tau' - [\tau_p^\phi - \tau -]_M - \tau' -$) comprising two DANTE combs, both with $M = 10$, a delay between the two DANTE trains that may be set to $\tau' = 0$, and step the relative phase ϕ of the two D_{10}^ϕ blocks to refocus both chemical shifts and dipolar or quadrupolar interactions. To this effect, one must select the coherence transfer pathway (CTP) $p = 0 \rightarrow p = +1 \rightarrow p = -1$ [13]. The length τ_p of the individual pulses must be $\tau_p = \tau_{90^\circ}/M$, or, equivalently, their nutation angles must be $\beta = 2\pi\nu_1\tau_{90^\circ}/M = \pi/(2M)$. If the individual pulses have a cumulative effect, each D_{10} train corresponds to a $\pi/2$ pulse, and the $D_{10}^x - \tau' - D_{10}^\phi - \tau' -$ sequence is therefore equivalent to a $90_x^\circ - \tau - 90_\phi^\circ - \tau -$ solid echo sequence.

In order to understand the differences between static and spinning samples, we performed numerical simulations for a spin system comprising two equivalent dipolar-coupled $I = 1/2$ spins. Figure 1(b) shows a simulation of the behavior of
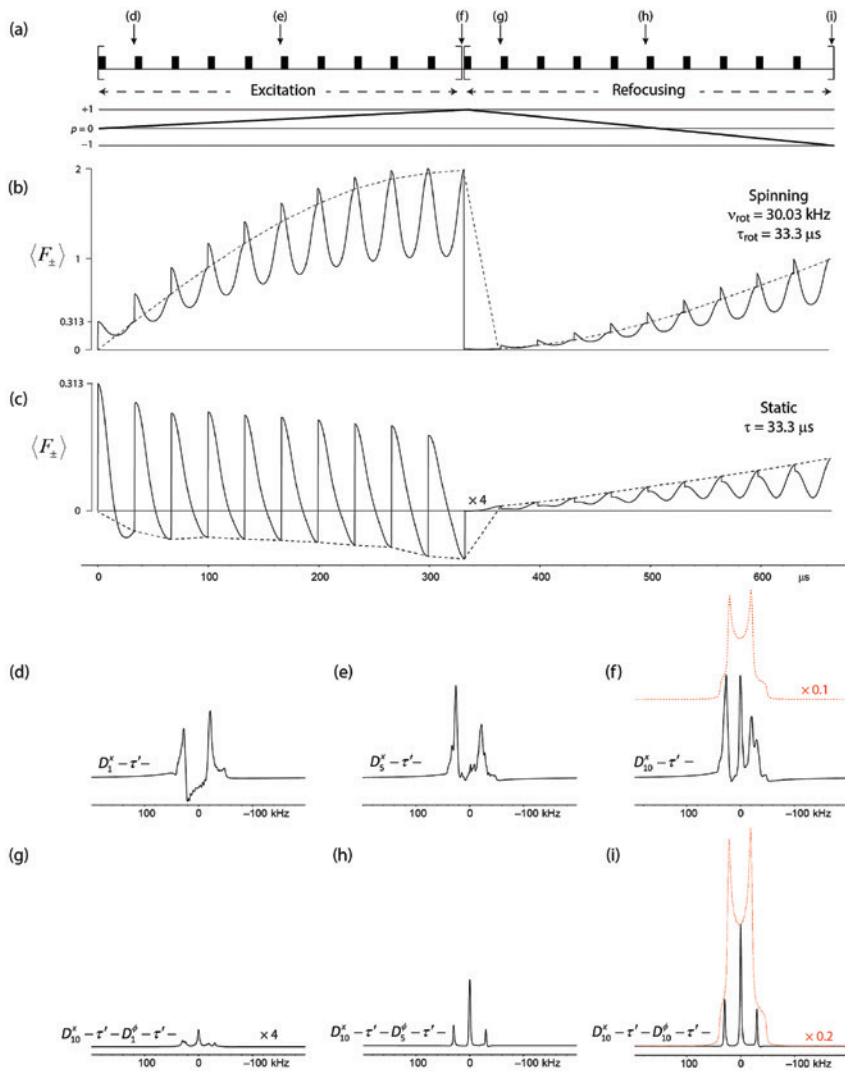
single-quantum (SQ) coherences $\langle I_{\pm}+S_{\pm}\rangle$ in a spinning sample in the course of the solid echo sequence $D_1^{10,x} - \tau' - D_1^{10,\phi} - \tau' -$ of Figure 1(a), with an rf-field strength $\nu_1 = 125$ kHz, $\tau_p = 0.2$ µs, $M = 10$, so that $M\tau_p = 10 \times \tau_p = \tau_{90°} = 2$ µs for each D_{10} block, $\tau_{rot} = 33.3$ µs corresponding to $\nu_{rot} = 1/\tau_{rot} = 30.03$ kHz, a delay between the two DANTE trains $\tau' = 0$, and intervals between adjacent pulses within each train of $\tau = \tau_{rot} - \tau_p = 33.1$ µs. Each D_{10} block lasts $10 \times (\tau + \tau_p) = 10 \times \tau_{rot} = 333$ µs. A chemical

Fig. 1: (a) Scheme representing a solid echo experiment comprising two D_{10} DANTE sequences for excitation and refocusing, i.e. either a $D_1^{10,x} - \tau' - D_1^{10,\phi} - \tau' -$ or $D_{10}^x - \tau' - D_{10}^\phi - \tau' -$ (with $\tau' = 0$) for spinning or static samples, respectively, with corresponding coherence transfer pathway (CTP) diagram. (b) and (c) Numerical simulations of the nutation of the magnetization during a $D_1^{10,x} - \tau' - D_1^{10,\phi} - \tau' -$ and $D_{10}^x - \tau' - D_{10}^\phi - \tau' -$ solid echo sequences for static and spinning samples, respectively. Dashed black lines indicate signal intensities when the acquisition is started at the end of each DANTE block in the course of the pulse sequence of (a). (d–i) Simulated spectra of spinning samples obtained by Fourier transformation of signals when the acquisition is started at the points indicated by black arrows in (a). The red lines in (f) and (i) show the ideal powder pattern of the static solid. The relevant parameters of the system with two equivalent dipolar-coupled protons are $d = -30$ kHz, $\nu_1 = 125$ kHz, $\tau_p = 0.2$ μs, $\tau' = 0$ and $\tau = 33.1$ μs. A chemical shift anisotropy characterized by $\delta_{iso} = 0$ ppm, $\Delta_{aniso} = -10$ ppm and $\eta = 0.9$ was considered. The external field was $B_0 = 9.4$ T and the principal components of the shielding and dipolar tensors were assumed to be parallel to one another. Powder averaging was performed over 2000 crystal orientations. Only the real parts of the echoes and spectra are shown. The spectra (d–f) result from the acquisition of $p = -1$ coherence. The first half of the nutation profiles of (b) and (c) result from the acquisition of $p = +1$ coherence, in accordance with the coherence transfer pathway of (a). The second half of the nutation profile of (c) has been expanded vertically by a factor 4 for clarity.

shift anisotropy (CSA) characterized by $\delta_{iso} = 0$ ppm, $\Delta_{aniso} = -10$ ppm and $\eta = 0.9$ was included. The external field was $B_0 = 9.4$ T (400 MHz for protons) and 2000 crystal orientations were considered. For simplicity, the main axes of the shielding and dipolar tensors were assumed to be parallel to one another. All interactions are active during both intervals and rf pulses. In contrast to previous studies, we followed the coherences throughout the entire echo sequence. In the nutation profiles, a boost in signal intensity amounts to an increase of the observable SQ coherence or transverse magnetization. Coherence transfer selection may be imposed by Exorcycle [15], i.e. by incrementing the phase $\phi = n\Delta\phi$ (with $n = 0, 1, 2, 3$ and $\Delta\phi = \pi/2$) of the second $D_1^{10,\phi}$ refocusing train, while alternately adding and subtracting the signals. As has been shown elsewhere for the excitation [6], each pulse acts on a rotational echo so that a cumulative effect is observed, generating the full signal intensity corresponding to a 90° pulse, i.e. at the end of the first $D_1^{10,x}$ DANTE train $\langle F_- \rangle = Tr[\rho(t)F_-] = 2$, where $\langle F_\pm \rangle = \langle I_\pm + S_\pm \rangle$. The second $D_1^{10,\phi}$ block leads to a build-up of coherence with order $p = -1$ by conversion from the coherence with order $p = +1$ generated by the first $D_1^{10,x}$ block, owing to the cumulative effect. Half-way during the sequence, provided coherence selection by phase cycling ensures that $p = +1 \rightarrow p = -1$, the signal drops to zero. This is due to the fact that $p = +1$ coherence (i.e. $\langle F_- \rangle$) is selected during the first half of the echo whereas $p = -1$ (i.e. $\langle F_+ \rangle$) is selected during the second half of the echo. In other words, no $p = -1$ coherence is present after the first block $D_1^{10,x}$, since phase cycling cancels

this coherence order. In contrast, during the second block $D_1^{10,\phi}$, $p = -1$ coherence is generated from the $p = +1$ coherence selected during the first block. At the end of the second $D_1^{10,\phi}$ block, the signal intensity is $Tr[\rho(t)F_+] = 1$, i.e. half of what was obtained after the first $D_1^{10,x}$ block. This stems from the fact that we consider a solid echo rather than a Carr–Purcell echo. The dashed line in Figure 1(b) passes through points at which the acquisition of FID's could by started (just before each pulse in the train) and indicates how the signal intensity of the resulting spectra would vary during such hypothetical experiments.

Figure 1(c) shows a profile analogous to that of Figure 1(b) that one obtains for a static non-spinning sample with the sequence $D_{10}^x - \tau' - D_{10}^\phi - \tau' -$ with a delay between the two DANTE trains $\tau' = 0$. During the first D_{10}^x train, as expected, no cumulative effect is observed since there are no rotational echoes. In the intervals between the pulses, the inhomogeneous interaction causes a dephasing of the $p = +1$ coherence and each pulse acts on partially dephased coherences, which, in contrast to spinning samples, results in a failure to build up any signal. As one can appreciate from Figure 1(b) and (c), the signal intensity created by the first pulse is $Tr[\rho(t)F_-] = 0.31$ in both spinning and static samples.

Surprisingly, after the $p = +1 \rightarrow p = -1$ transfer, half-way during the sequence, one observes a completely different profile, with a cumulative effect that leads to a build-up of the signal similar to that of the spinning case. In the intervals between the pulses, one observes an increase in signal intensity. This is solely due to free evolution under inhomogeneous interactions and merely resembles the refocusing effect due to the mechanical rotation observed in the spinning case of Figure 1(b). The dashed line has the same meaning as in Figure 1(b). It is interesting to note that, in contrast to the spinning case, where each pulse leads to a signal increase, in the static case each pulse results in a loss of signal during the second refocusing train. This decrease in intensity is however compensated by the above-mentioned increase due to the free evolution under the shift and dipolar interactions, resulting in a cumulative effect. In contrast to the spinning case, where the cumulative build-up is due to the action of the rf pulses, in the static case the cumulative build-up during the second half of the echo is due to the refocusing of inhomogeneous broadenings ensured by coherence pathway selection. At the end of the $D_{10}^x - \tau' - D_{10}^\phi - \tau' -$ sequence, the signal intensity is $Tr[\rho(t)F_+] = 0.03$ in a static sample. Compared to the ideal fully refocused echoes that can be obtained in samples spinning about the magic angle, where the expectation value of the coherence at the top of the echo is 100%, the fraction that can be refocused in static samples is only 3% in the spin system under investigation with our estimate of the average over all crystallite orientations in the powder. The profile of Figure 1(b) corresponding to the second refocusing train of pulses has been amplified by a factor 4.

Figure 1(d–f) show, from left to right, the static spectra which would result if one started the signal acquisition directly after excitation (without refocusing), e.g. after pulse trains (d) $D_1^x - \tau' -$, (e) $D_5^x - \tau' -$ or (f) $D_{10}^x - \tau' -$ (with $\tau' = 0$), as indicated by black arrows in Figure 1(a). The spectra are highly distorted as a result of the dephasing that occurs during the τ intervals between pulses. A simulation of an ideal Pake pattern is overlaid in (f) with a vertical scaling factor. Figure 1(g–i) show, from left to right, the spectra that would result if one acquired the signal after 'truncated' spin echo sequences (g) $D_{10}^x - \tau' - D_1^\phi - \tau' -$, (h) $D_{10}^x - \tau' - D_5^\phi - \tau' -$ and (i) $D_{10}^x - \tau' - D_{10}^\phi - \tau' -$, respectively, as indicated by black arrows in Figure 1(a) (with $\tau' = 0$). From left to right, one can appreciate the increase in signal intensity as the second DANTE train approaches a cumulative nutation angle of 90°. The spectrum of Figure 1(i) results from a complete $D_{10}^x - \tau' - D_{10}^\phi - \tau' -$ solid echo sequence. As expected, one observes three peaks corresponding to three rf spikelets spaced by $1/\tau = 30.03$ kHz. Their envelope can be compared with the ideal static Pake pattern (red line) which extends over *ca.* 100 kHz. The intensities of the three peaks nicely reproduce that of the envelope of the static powder pattern.

In order to obtain insight into the spin dynamics during a DANTE echo sequence applied to a static sample, we shall consider the shortest possible DANTE sequence $D_2^x - \tau' - D_2^\phi - \tau' -$ that can be seen as analogous to a solid echo. For the sake of comparison with the ideal case of a complete refocusing, the MAS condition will also be considered. A scheme depicting the pulse sequence, with its corresponding CTP, is shown in Figure 2(a), for $\tau' = 0$. The relevant state of the system is indicated by the index (n). We chose a model system comprising two equivalent ^{1}H spins with a homonuclear dipolar coupling $d = -10$ kHz, appropriate for a single crystal with a dipolar tensor perpendicular to the external magnetic field, and ideal pulses with flip angles $\beta = \pi/4$ and delays between the pulses $\tau = 100$ μs. No shift interaction was included for simplicity. The profiles obtained, assuming proper selection of the change in coherence order, are shown in Figure 2(b) with black and red lines for spinning ($\nu_{rot} = 10$ kHz) and static samples, respectively. Even with these drastic simplifications, the peculiar features highlighted in the profile of Figure 1(c) are preserved, i.e. the dephasing during the first train with $p = 0 \rightarrow p = +1$, the rephasing effect during the second train with $p = +1 \rightarrow p = -1$ and the ability of the dipolar interaction to increase the signal intensity under free evolution. This latter feature may be seen as a partial refocusing of the internal interactions. We monitored the relevant SQ matrix elements before and after each rf pulse and at the end of the echo, as indicated by numbers in brackets in Figure 2(a). The state of the system at point (n) of the pulse sequence is described by $\rho(n) = U_\lambda \rho(n-1) U_\lambda^\dagger$, with the propagator $U_\lambda = \exp(-iH_\lambda \tau)$ for the interaction λ, which can be either an rf-pulse or a dipolar coupling, described either by the
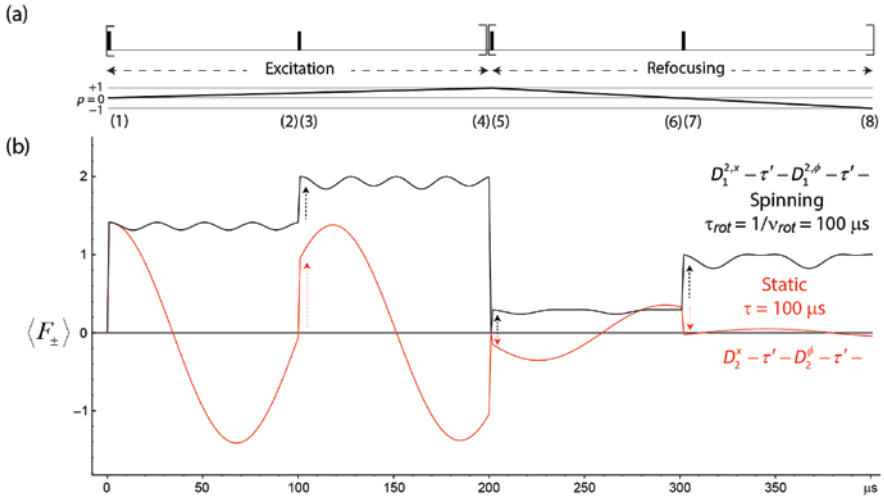
(a)

(b)

Fig. 2: (a) Scheme representing a solid echo experiment comprising two D_2 DANTE sequences, with corresponding coherence transfer pathway diagram. (b) Numerical simulations of the experiment shown in (a) for spinning $(D_1^{2,x} - \tau' - D_1^{2,\phi} - \tau' -)$ or static samples $(D_2^x - \tau' - D_2^\phi - \tau' -)$, in black and red, respectively. The relevant parameters of the system consisting of two equivalent dipolar-coupled ^{1}H nuclei are $d = -10$ kHz, $\nu_1 = 125$ kHz, $\tau_p = 1\,\mu$s, $\tau = 100\,\mu$s and $\tau' = 0$. All pulses are considered to be ideal. Simulations were performed assuming one single crystal, with a dipolar tensor perpendicular to the external magnetic field B_0. Only the real parts of the relevant expectation values are shown.

Hamiltonian $H_{rf} = \omega_1(F_x \cos\phi + F_y \sin\phi)$ or by $H_D = -(d/2)\ (3\cos^2\theta - 1)(3I_zS_z - IS)$. Since we make use of ideal (infinitely short) pulses, no interaction other than the rf pulse can take place between states (2) and (3). Therefore, rather than 'at time (n)', we shall speak of 'at point (n)' of the pulse sequence shown in Figure 2(a). In the spinning case, at points (2), (4), (6) and (8), a rotational echo is formed and the dipolar interaction is fully refocused by the mechanical rotation and can therefore be completely ignored. Therefore, in the spinning case it can be shown that $\langle F_-\rangle_{(1)} = \langle F_-\rangle_{(2)} = \sqrt{2}$, $\langle F_-\rangle_{(3)} = \langle F_-\rangle_{(4)} = 2$, $\langle F_+\rangle_{(5)} = \langle F_+\rangle_{(6)} = 1 - 1/\sqrt{2}$ and $\langle F_+\rangle_{(7)} = \langle F_+\rangle_{(8)} = 1$. In the static case, on the other hand, one finds the following expressions:

$$\langle F_-\rangle_{(1)} = \sqrt{2} \tag{1}$$

$$\langle F_-\rangle_{(2)} = \sqrt{2}\cos\left(\frac{3\tau d}{4}\right) \tag{2}$$

$$\langle F_-\rangle_{(3)} = 1 + \cos\left(\frac{3\tau d}{4}\right) \tag{3}$$

$$\langle F_-\rangle_{(4)} = \cos\left(\frac{3\tau d}{4}\right) + \cos\left(\frac{3\tau d}{2}\right) \tag{4}$$

$$\langle F_+\rangle_{(5)} = -\frac{1}{4}(\sqrt{2}-2)\left[\cos\left(\frac{3\tau d}{4}\right) + \cos\left(\frac{3\tau d}{2}\right)\right] \tag{5}$$

$$\langle F_+\rangle_{(6)} = \frac{1}{4}\left[1 + \cos\left(\frac{3\tau d}{4}\right) - (\sqrt{2}-1)\cos\left(\frac{3\tau d}{2}\right) - (\sqrt{2}-1)\cos\left(\frac{9\tau d}{4}\right)\right] \tag{6}$$

$$\langle F_+\rangle_{(7)} = \cos^2\left(\frac{3\tau d}{8}\right)\cos\left(\frac{3\tau d}{4}\right) \tag{7}$$

$$\langle F_+\rangle_{(8)} = \frac{1}{2}\cos^2\left(\frac{3\tau d}{8}\right)\left[\cos\left(\frac{3\tau d}{4}\right) + \cos\left(\frac{3\tau d}{2}\right) + 2\sin^2\left(\frac{9\tau d}{8}\right)\right]. \tag{8}$$

The numerical values of these expectation values are given in Table 1 for $d = 10$ kHz, $\tau_p = 1$ μs and intervals between pulses $\tau = 100$ μs $- \tau_p = 99$ μs. Equation 8 reveals that the dipolar interaction is not fully refocused at the end of a DANTE solid echo sequence. The rf pulses in the second refocusing DANTE train have different effects under spinning and static conditions, i.e. in the spinning case, the rf pulses lead to an increase of $\langle I_+\rangle$ whereas, in the static case, the rf pulses result in a decrease of SQ coherence. This can be estimated by the variation of the relevant expectation values between points (4) and (5) $\Delta\langle F_+\rangle_{(5,4')} = 0.2929$ and -0.1527, for spinning and static cases, respectively,

Tab. 1: Expectation values of relevant operators at selected points in the pulse sequence $D_2^x - \tau' - D_2^\phi - \tau' -$ of Figure 2, evaluated using Equations (2–8). The relevant parameters are $d = -10$ kHz, $\nu_1 = 125$ kHz, $\tau_p = 1$ μs, $\tau = 100$ μs $- \tau_p = 99$ μs and $\tau' = 0$. Pulses are considered as ideal with a vanishing duration. A single crystal is assumed, with the principal axis of the dipolar tensor perpendicular to the external magnetic field B_0.

$\langle F_\pm\rangle_{(n)}$	Spinning	Static
(1)	$\sqrt{2}$	$\sqrt{2}$
(2)	$\sqrt{2}$	−0.0667
(3)	2	0.9529
(4)	2	−1.0427
(4′)	0	0
(5)	$1-1/\sqrt{2}$	−0.1527
(6)	$1-1/\sqrt{2}$	0.3267
(7)	1	−0.0224
(8)	1	−0.0437

or between points (6) and (7) $\Delta\langle F_+\rangle_{(7,6)} = 0.7071$ and -0.3491, for spinning and static cases, respectively. These effects are highlighted by dashed arrows in Figure 2(b). Therefore, the descriptor $\Delta\langle F_+\rangle_{(n,n-1)}$ evaluated during rf pulses in the second DANTE train of the solid echo sequence is always positive under MAS and always negative in static samples. During the first DANTE train of the echo sequence, on the other hand, $\Delta\langle F_-\rangle_{(n,n-1)}$ is always positive during the pulses in both spinning and static samples. Furthermore, and only during the second refocusing train of rf pulses, the inhomogeneous dipolar interaction increases the projection onto the transverse plane during free evolution in static samples. This can be appreciated between points (5) and (6), where one finds $\Delta\langle F_+\rangle_{(6,5)} = 0.4794$. By contrast, in the intervals between rf pulses, this descriptor always vanishes under MAS, since two consecutive points, say (5) and (6), correspond to tops of rotational echoes, where all inhomogeneities are refocused. In the single-crystal case of Figure 2(b), and in contrast to what was observed in the powder average of Figure 1(b), the last free evolution interval between (7) and (8) results in $\Delta\langle F_+\rangle_{(8,7)} = -0.0213$. This is in disagreement with what can be seen between points (5) and (6). However, we find that, when extensive powder averaging is performed, the descriptor $\Delta\langle F_+\rangle_{(n,n-1)}$ evaluated in the intervals between rf pulses is always positive in static samples during the second train of a DANTE solid echo sequence. This latter feature is ensured by coherence transfer selection and reflects the partial refocusing effect of the second DANTE pulse train.

Figure 3(a) shows an experimental solid-echo spectrum of the protons of water in a static sample of barium chlorate monohydrate ($BaClO_3.H_2O$). An almost ideal Pake pattern is observed, thus confirming, as discussed above, that intermolecular dipolar couplings can be neglected and that the two-spin system can be assumed to be isolated. The asymmetry in the shoulders of the pattern (the low-frequency or right-hand side being more pronounced than the high-frequency side) is due to the shielding anisotropy of the protons. Figure 3(b–d), show solid echo spectra obtained with different spin-echo sequences $D_5^x - \tau' - D_5^\phi - \tau' -$, $D_{10}^x - \tau' - D_{10}^\phi - \tau' -$ and $D_{20}^x - \tau' - D_{20}^\phi - \tau' -$ of the same sample as in Figure 3(a). As the rf field strength was $\nu_1 = 114$ kHz, the lengths of the individual pulses were chosen to be $\tau_p = 0.44$, 0.22 and 0.11 µs, corresponding to cumulative nutation angles of $\beta = \pi/2$ in all cases ($0.44 \times 5 = 0.22 \times 10 = 0.11 \times 20 = 2.2$ µs). The delays between the pulses were $\tau = 56.60$, 31.30 and 12.10 µs, respectively, corresponding after Fourier transformation to excitation profiles with rf spikelets spaced by 17.5, 31.9 and 81.9 kHz, respectively. The delay between the two DANTE trains was $\tau' = 0$ in all cases. As previously highlighted by the simulations of Figure 1, at the end of the solid echo sequences, the DANTE trains indeed allow one to acquire reasonably undistorted lineshapes in static samples. These spectra show that, by
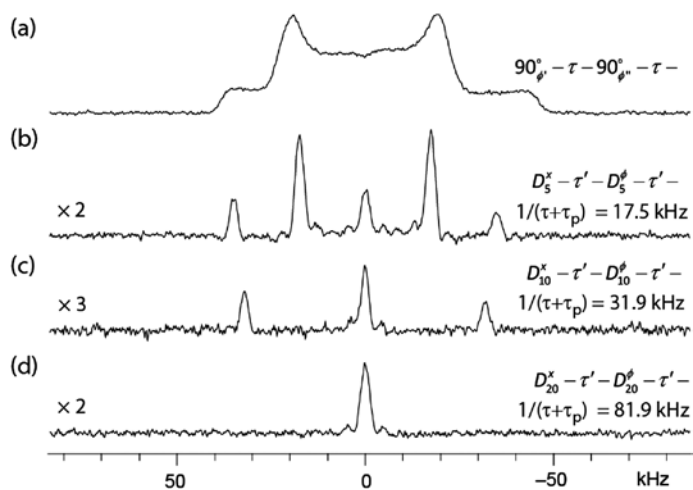
Fig. 3: (a) Experimental static lineshape due to pairs of dipolar-coupled protons in a static non-spinning sample of barium chlorate monohydrate, obtained by Fourier transformation of the decaying half of a solid echo excited by a conventional $90° - \tau - 90° - \tau$ sequence with 90° pulses of 2.2 μs duration and $\tau = 50$ μs. (b–d) Spectra obtained by Fourier transformation of the decaying halves of solid echoes excited by DANTE sequences (b) $D_5^x - \tau' - D_5^\phi - \tau' -$, (c) $D_{10}^x - \tau' - D_{10}^\phi - \tau' -$ and (d) $D_{20}^x - \tau' - D_{20}^\phi - \tau' -$ with $\tau' = 0$, $\tau + \tau_p = 57.04$, 31.52 and 12.21 μs, respectively. The pulse lengths were $\tau_p = 0.44$, 0.22 and 0.11 μs, respectively, with a strong rf-field $\nu_1 = 114$ kHz.

means of DANTE pulse trains, one can selectively excite 'slices' across an inhomogeneous lineshape. This amounts to say that a chosen 'window' of crystallite orientations within a powder pattern can be selectively excited and explored.

Figure 4 shows experimental spectra analogous to those of Figure 3, with the exception that a roughly 4-fold weaker rf-field strength of $\nu_1 = 26$ kHz ($\tau_{90°} = 9.6$ μs) was used in a solution-state NMR spectrometer. The lower rf amplitude leads to the slightly distorted powder pattern of Figure 4(a), where the shoulders of the Pake pattern are less pronounced compared to those of Figure 3(a). On the other hand, the DANTE spectra of Figure 4(b–d) obtained with $\nu_1 = 26$ kHz are substantially identical to those of Figure 3(b–d), obtained $\nu_1 = 114$ kHz. Subtle differences in the relative intensities of the peaks of Figures 3 and 4 are ascribed to variations in T_1 observed for crystallites of $BaClO_3.H_2O$ with different orientations [15] bearing in mind that different recovery delays of 5 and 10 s were used in the experiments of Figures 3 and 4. These observations confirm that DANTE echo trains may be used to excite and refocus inhomogeneously broadened lines with line widths that greatly exceed the strength of the rf field [6].
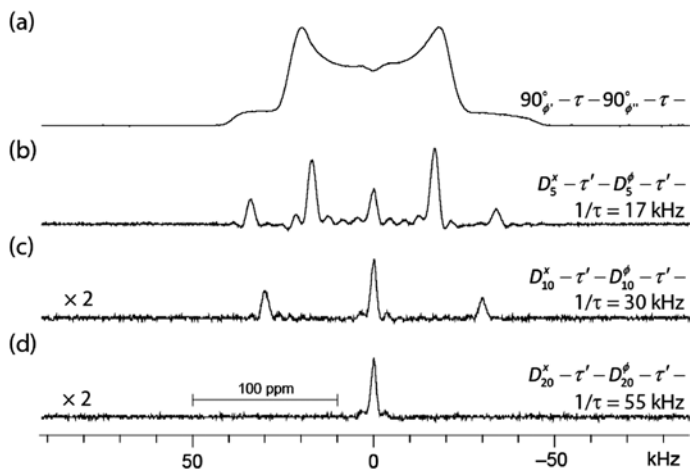
(a)

$90°_{\phi'} - \tau - 90°_{\phi''} - \tau -$

(b)

$D^x_5 - \tau' - D^\phi_5 - \tau' -$
$1/\tau = 17$ kHz

(c)

× 2

$D^x_{10} - \tau' - D^\phi_{10} - \tau' -$
$1/\tau = 30$ kHz

(d)

× 2

100 ppm

$D^x_{20} - \tau' - D^\phi_{20} - \tau' -$
$1/\tau = 55$ kHz

50   0   −50   kHz

Fig. 4: (a) Experimental static lineshape due to pairs of dipolar-coupled protons in a static non-spinning sample of barium chlorate monohydrate, obtained by Fourier transformation of the decaying half of a solid echo excited by a conventional $90°_x - \tau - 90°_y - \tau -$ sequence with 90° pulses of 9.6 μs duration and $\tau = 50$ μs. (b−d) Spectra obtained by Fourier transformation of the decaying halves of solid echoes excited by DANTE sequences (b) $D^x_5 - \tau' - D^\phi_5 - \tau' -$, (c) $D^x_{10} - \tau' - D^\phi_{10} - \tau' -$ and (d) $D^x_{20} - \tau' - D^\phi_{20} - \tau' -$ with $\tau' = 0$, and $\tau + \tau_p = 58.82$, 33.33 and 18.18 μs, respectively. The pulse lengths were $\tau_p = 1.92$, 0.96 and 0.48 μs, respectively, with a weak rf-field strength $\nu_1 = 26$ kHz. The recycling delay was 10 s in all cases. Sixteen transients were averaged in (a) whereas 32 scans were acquired in (b−d). The carrier frequency was set to 0 Hz in all cases. No line broadening was applied.

When dealing with an isolated dipolar-coupled spin pair, as in our case, each single crystal gives rise to a doublet with a splitting determined by the magnitude of the coupling constant d and the angle θ subtended between the main axis of the dipolar tensor and the external magnetic field. The two transitions of the doublet have frequencies $\nu^D_\pm(\theta) = \delta_{iso} \pm 3d(3\cos^2\theta - 1)/4$ where δ_{iso} is the chemical shift, assumed to be isotropic. It is worth bearing in mind at this point that each single transition of the doublet is 'shared' by each of the two spins. In fact, if one could detect only one of the two protons, one would obtain exactly the same Pake pattern with half the intensity, i.e. $\langle F_\pm(t)\rangle = 2\langle I_\pm(t)\rangle = 2\langle S_\pm(t)\rangle$. The splitting is maximum when $\theta = 0°$, i.e. $\Delta\nu^D(0) = 3d$, vanishes at the magic angle $\theta = 54.7°$, and becomes negative for $\theta = 90°$, $\Delta\nu^D(\pi/2) = -3d/2$. Between the inner 'horns' of the pattern, each doublet can correspond to two different orientations. By contrast, outside these 'horns', near the 'shoulders', each doublet corresponds to a crystallite with a unique orientation. One can choose the parameters of a DANTE static echo sequence so as to obtain spectra that correspond either to a unique or to two

crystal orientations by setting the carrier frequency ν_{rf} and the delay τ between adjacent pules according to:

$$\nu_{rf}(\theta) = \nu_{\pm}^{D}(\theta) = \delta_{iso} \pm \frac{3}{4} d(3\cos^2\theta - 1) \tag{9}$$

$$\tau(\theta)^{-1} = \frac{3}{2} d(3\cos^2\theta - 1). \tag{10}$$

A system made up of a single isolated spin $S = 1/2$, subject to an anisotropic interaction such as a chemical shift anisotropy, would produce a powder line-shape made up of a single peak (rather than a doublet) for each crystal orienta-tion. In such cases, each peak resulting from a DANTE echo can be ascribed to a single crystallite orientation. Thus DANTE-based techniques allow one to detect a subspectrum corresponding to a particular range of crystallite orientations. In spectra such as those shown in Figures 3(b–d) and 4(b–d), one expects a range of crystallite orientations to contribute to the signal. The 'purity' of DANTE signals in terms of the number of crystallites that contribute depends on the width of the rf spikelets resulting from the DANTE trains. This width is determined by the total length of the rf sequence and, in the case of the solid echoes used in this work, is proportional to $(2\,M\tau)^{-1}$.

Figure 5 shows spectra which demonstrate how DANTE echoes may be tuned so as to explore particular sets of crystallite orientations. In Figure 5(a), the static pattern obtained with a conventional solid echo is shown to guide the eye. Figure 5(b) shows that a 'horns-only' DANTE spectrum may be obtained by an appropriate choice of the carrier frequency and pulse interval. Figure 5(c) shows that a 'single-horn' spectrum may be obtained simply by decreasing the pulse intervals used in (b). Figure 5(d) shows a 'shoulders-only' spectrum of the Pake pattern of Figure 5(a). Near the shoulders, doublets associated with single-crys-tallite orientations may be explored. A 'single-shoulder' spectrum is shown in Figure 5(e). In the latter case, a single transition of a doublet associated with a single crystal is excited. The carrier frequency is indicated by black arrows when different from 0 Hz.

The necessity to resort to a second DANTE train for refocusing is demon-strated in Figure 6. In (a), a spectrum obtained with a $D_{10}^{x} - \tau' - D_{10}^{\phi} - \tau' -$ echo is shown. This is in very good agreement with the simulation of Figure 1(i). Figure 6(b) shows the spectrum resulting from a single $D_{10}^{x} - \tau' -$ train, i.e. when no refocusing train is used. The lineshape obtained in the latter case is character-ized by distortions that are in very good agreement with the simulations shown in Figure 1(f). The partial failure to refocus the dipolar interactions in static samples at the end of a DANTE solid echo sequence results in distortions of the spectra that
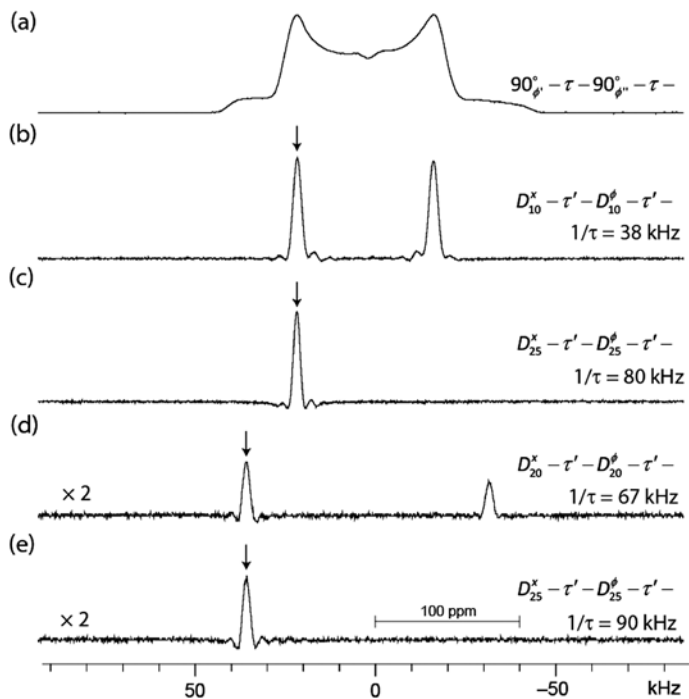
Fig. 5: (a) Experimental static lineshape as in Figure 3(a) shown for comparison. (b–e) Spectra obtained by Fourier transformation of the decaying halves of solid echoes excited by DANTE sequences (b) $D_5^x - \tau' - D_5^\phi - \tau' -$, (c) $D_{10}^x - \tau' - D_{10}^\phi - \tau' -$, (d) $D_{20}^x - \tau' - D_{20}^\phi - \tau' -$ and (e) $D_{25}^x - \tau' - D_{25}^\phi - \tau' -$ with $\tau' = 0$, and $\tau + \tau_p = 26.32, 12.50, 14.93$ and $11.11\ \mu s$, respectively. The pulse lengths were $\tau_p = 0.96, 0.38, 0.48$ and $0.38\ \mu s$, respectively, with a weak rf-field $\nu_1 = 26\ kHz$. The recycling delay was 10 s in all cases. Sixteen transients were averaged in (a) whereas 32 scans were acquired in (b–e). The carrier frequency was set to 0 Hz in (a) and is indicated by black arrows in all other cases. No line broadening was applied.

are analogous to those obtained if one inserts a long 'dead time' before starting signal acquisition. However, as may be appreciated in the experimental spectra of Figures 3(b–d) and 4(b–d), the extent of dephasing is perfectly acceptable in our case.

3 Conclusions

We have analyzed the response to DANTE trains of rf pulses applied to static samples in solid-state NMR spectroscopy. In contrast to MAS experiments, where
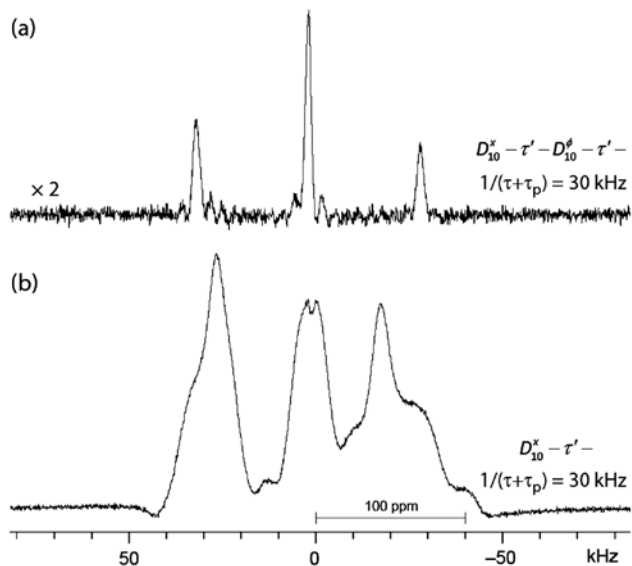
Fig. 6: (a) Experimental static lineshape obtained with a sequence $D_{10}^x - \tau' - D_{10}^\phi - \tau' -$ as in Figure 4(c) shown for comparison. (b) Experimental spectrum resulting from a single DANTE sequence $D_{10}^x - \tau' -$ used for direct excitation, without resorting to a second $D_{10}^\phi - \tau' -$ train for refocusing, with $\tau + \tau_p = 33.33$ μs, $\tau' = 0$ and $\tau_p = 0.96$ μs, with a weak rf-field $v_1 = 26$ kHz. The recycling delay was 10 s and 16 transients were averaged in all cases. The carrier frequency was set to 0 Hz in both (a) and (b). No line broadening was applied. Zero-th and first-order phase corrections were −303 and 308, and −288 and 308°, in (a) and (b), respectively.

it is possible to use a single rotor-synchronized DANTE train for direct excitation without resorting to refocusing, in static samples one can only obtain reasonably undistorted lineshapes if one uses spin echoes that are refocused by a second DANTE pulse train. This has been shown both by numerical simulations and by experiments performed on the protons of hydration water in barium chlorate monohydrate. The spectral bandwidths that one can access with DANTE techniques in static samples open up new ways for exploring the responses of selected crystallites in powder samples.

4 Experimental details

A sample of *ca.* 50 mg $Ba(ClO_3)_2.H_2O$ (Alfa Aesar) was kept under vacuum (ca. 10 Pa) overnight prior to the experiments in order to minimize the adsorbtion

of water which leads to a sharp isotropic peak in the middle of the Pake pattern. All ^{1}H spectra of Figure 3 excited with "hard" rf pulses have been recorded at the EPFL on a Bruker 400 spectrometer (9.4 T) with an Avance-II console, using 3.2 mm rotors in a triple resonance MAS probe designed for low-temperature measurements near 100 K, but used at room temperature without microwave irradiation and without spinning. The rf-field amplitude was $\nu_1 = 114$ kHz. A recycling delay of 5 s was used. All ^{1}H spectra of Figures 4–6 excited with "soft" rf pulses have been recorded at the University of Neuchâtel on a Bruker 400 spectrometer (9.4 T) with an Avance-II console, using 5 mm tubes in a triple resonance probe designed for solution-state NMR. The rf-field amplitude was $\nu_1 = 26$ kHz. A recycling delay of 10 s was used. All solid echoes were phase cycled for the selection of the $p = 0 \rightarrow p = 1 \rightarrow p = -1$ pathway by nesting Exorcycle [16] and Cyclops [17] to produce an overall 16-step phase cycle. The delay between the two DANTE trains was $\tau' = 0$, in all cases. Numerical simulations were performed with SIMPSON [18], using 2000 crystal orientations sampled with the REPULSION scheme [19].

References

1. M. J. Duer, Solid-State NMR Spectroscopy: Principles and Applications, Blackwell Science, UK, (2002).
2. G. Bodenhausen, R. Freeman, G. A. Morris, J. Magn. Reson. **23** (1976) 171.
3. P. Caravatti, G. Bodenhausen, R. R. Ernst, J. Magn. Reson. **55** (1983) 88.
4. V. Vitzthum, M. A. Caporini, S. Ulzega, G. Bodenhausen, J. Magn. Reson. **212** (2011) 234.
5. V. Vitzthum, M. A. Caporini, S. Ulzega, J. Trébosc, O. Lafon, J. -P. Amoureux, G. Bodenhausen, J. Magn. Reson. **223** (2012) 228.
6. D. Carnevale, V. Vitzthum, O. Lafon, J. Trébosc, J. -P. Amoureux, G. Bodenhausen, Chem. Phys. Lett. **553** (2012) 68.
7. D. Carnevale, A. J. Perez Linde, G. Bauer, G. Bodenhausen, Chem. Phys. Lett. **580** (2013) 172.
8. X. Lu, J. Trébosc, O. Lafon, D. Carnevale, S. Ulzega, G. Bodenhausen, J. -P. Amoureux, J. Magn. Reson. **236** (2013) 105.
9. G. E. Pake, J. Chem. Phys. **16** (1948) 327.
10. D. Carnevale, S. E. Ashbrook, G. Bodenhausen, RSC Adv. **4** (2014) 56248.
11. J. G. Powles, P. Mansfield, Phys. Lett. **2** (1962) 58.
12. J. G. Powles, J. H. Strange, Proc. Phys. Soc. **82** (1963) 6.
13. S. Antonijevic, S. Wimperis, J. Magn. Reson. **164** (2003) 343.

14. G. Bodenhausen, H. Kogler, R. R. Ernst, J. Magn. Reson. **58** (1984) 370.
15. J. R. Long, R. Ebelhäuser, R. G. Griffin, J. Phys. Chem. A **101** (1997) 988.
16. G. Bodenhausen, R. Freeman, D. L. Turner, J. Magn. Reson. **27** (1977) 511.
17. D. I. Hoult, R. E. Richards, Proc. Roy. Soc. (London) **A344** (1975) 311.
18. M. Bak, J. T. Rasmussen, N. C. Nielsen, J. Magn. Reson. **147** (2000) 296.
19. M. Bak, N. C. Nielsen, J. Magn. Reson. **125** (1997) 132.